This is an open access article published under an ACS AuthorChoice License, which permits copying and redistribution of the article or any adaptations for non-commercial purposes.

ACS OMEGA

Article

Cite This: ACS Omega 2018, 3, 17629−17636

http://pubs.acs.org/journal/acsodf

Wettability, Photoactivity, and Antimicrobial Activity of Glazed Ceramic Tiles Coated with Titania Films Containing Tungsten

Diego Onna,*[,†,‡] Keyla M. Fuentes,*[,†] Cecilia Spedalieri,[†] Mercedes Perullini,[†] María Claudia Marchi,[†,∥] Fernando Alvarez,[⊥] Roberto J. Candal,[#] and Sara A. Bilmes*[,†]

[†]Instituto de Química Física de los Materiales, Medio Ambiente y Energía (INQUIMAE-CONICET), Departamento de Química Inorgánica, Analítica y Química Física (DQIAQF), Facultad de Ciencias Exactas y Naturales, Universidad de Buenos Aires, Ciudad Universitaria, Pabellón 2, C1428EHA Ciudad Autónoma de Buenos Aires, Argentina

[‡]Instituto de Nanosistemas, Universidad Nacional de General San Martín, CP1650 San Martín, Provincia de Buenos Aires, Argentina

[∥]Centro de Microscopías Avanzadas, Instituto de Física de Buenos Aires (IFIBA-CONICET), Universidad de Buenos Aires, C1428EHA Ciudad Autónoma de Buenos Aires, Argentina

[⊥]Instituto de Física "Gleb Wataghin", Universidade Estadual de Campinas (UNICAMP), Campinas, São Paulo 13083-970, Brazil

[#]Instituto de Investigación e Ingeniería Ambiental (3iA-CONICET), Universidad Nacional de San Martín, CP1650 San Martín, Provincia de Buenos Aires, Argentina

Supporting Information

ABSTRACT: Self-cleaning coatings are advanced materials for the removal of pollutants and microorganisms by combining wettability, photocatalytic degradation, and antimicrobial activity. In this work, we propose a rational design of self-cleaning films based on TiO_2 synthesized by sol−gel on commercial glazed ceramic tiles for building's indoor applications. The synthesis strategy is based on hydrolysis and condensation of Ti-isopropoxide in the presence of W(VI) precursors to tune defects and crystallinity of the resulting W−TiO_2 thin film. From the microstructure and surface composition analysis for different tungsten contents and annealing temperatures, we conclude that the film is composed by sintered TiO_2 particles with adsorbed polytungstates (WO_x) that inhibit anatase/rutile transformation. Polytungstates on TiO_2 also induce surface defects that enhance water contact angle and inactivation of *Escherichia coli* under visible light. The presence of W(VI) has a negligible effect toward crystal violet degradation either under visible or under UV light. These results provide evidence on the existence of at least two different types of defects: (i) intrinsic defect from a sol−gel route and (ii) induced defect by tungsten species on the surface. Understanding the correlation between composition, structure, and self-cleaning properties provides a base for an efficient design of low-cost self-cleaning ceramic tiles that can be fully manufactured in an industrial plant.

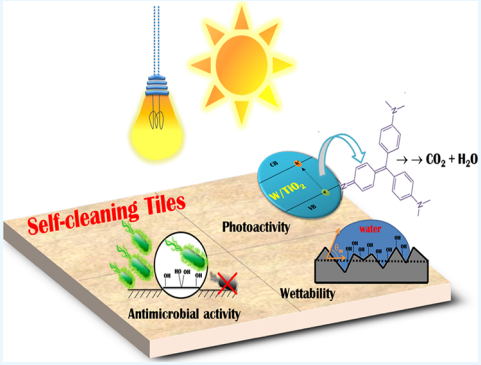

1. INTRODUCTION

The household cleaning usually requires sanitizing chemicals that potentially introduce hazardous compounds to the environment and human health.[1] To avoid these products, self-cleaning coatings represent a valuable and innovative strategy that triggered the design of advanced construction supplies.[2,3] The main requirements for these coatings are hydrophilicity for easy washing, efficient degradation of pollutants, and antimicrobial activity to reduce the need for chemical supplies.[4,5] Self-cleaning surfaces such as glass windows,[6] concrete blocks,[7] clay roofing tiles,[8] and ceramic glazed tiles[9] already exist in the market, but they are limited to high-end buildings as their final price is too high for a mass production market.

Titanium dioxide (TiO_2) is a widespread material whose properties are suitable for the fabrication of hydrophilic self-cleaning and antimicrobial surfaces, such as ceramic tiles.[10] Among its feature highlights, it is nontoxic, economically affordable, easy to deposit as thin films and exhibits good activity for pollutant photodegradation.[11] For designing self-cleaning tiles based on TiO_2 coatings, its electronic and crystalline structures should be controlled. For instance, the density of surface defects such as oxygen vacancies reduces the recombination rate of photogenerated electron−hole pairs (e−h) and introduces donor levels within the electronic structure of TiO_2, driving photoactivity in the visible range.[12] These defects might be induced by the synthesis pathway, especially on those sol−gel routes using organic precursors.[13] Defect

Received: November 29, 2018
Accepted: December 4, 2018
Published: December 18, 2018

Downloaded via UNIV NACIONAL DE SAN MARTIN on February 5, 2019 at 15:22:05 (UTC).
See https://pubs.acs.org/sharingguidelines for options on how to legitimately share published articles.

© 2018 American Chemical Society

DOI: 10.1021/acsomega.8b03339
ACS Omega 2018, 3, 17629−17636

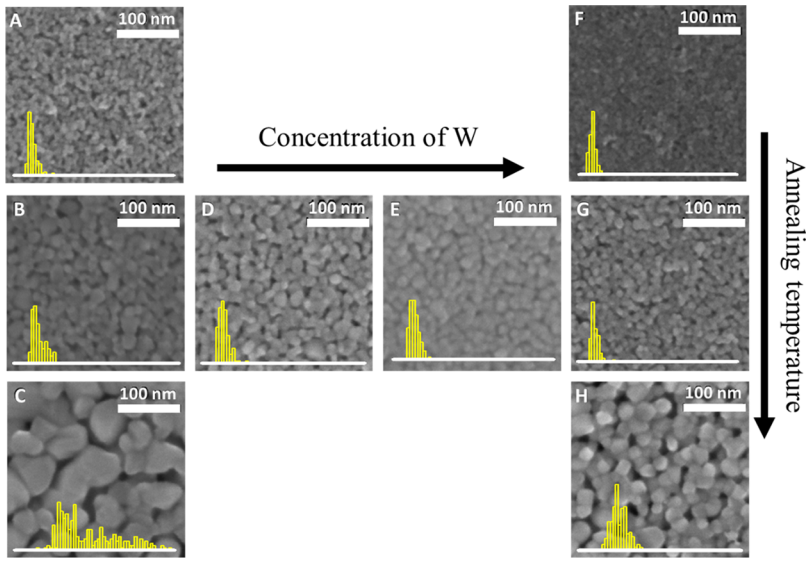

Figure 1. SEM images of the films for different W/Ti ratio and annealing temperatures. (A) W0 400 °C, (B) W0 600 °C, (C) W0 800 °C, (D) W1 600 °C, (E) W2 600 °C, (F) W5 400 °C, (G) W5 600 °C, and (H) W5 800 °C. Grain size distribution histogram for each sample is shown in the inset of the SEM images; in all cases, the scale bar for histograms is 120 nm.

density is further controlled by the subsequent thermal treatment. During thermal treatment, organic matter is removed, and TiO_2 nanoparticles dehydrate, coarsen, and crystallize. In particular, for $T > 600$ °C, the anatase to rutile transformation (ART) might occur, leading to photodegradation activity losses.[14]

The addition of foreign ions to TiO_2 is a common strategy for enhancing the TiO_2 self-cleaning properties.[15] However, ions must be carefully chosen to avoid lattice distortions inducing ART,[16,17] as well as defects in the TiO_2 matrix which can act as carrier recombination centers.[18] Among the possible ions, tungsten is a good candidate as it stabilizes the anatase phase at temperatures as high as 900 °C.[19] This is a key feature when considering these thin films for industrial applications because the tile manufacturing process requires high furnace temperatures.

Simultaneously, studies on photocatalysis, wettability, and antimicrobial activity on TiO_2-coated tiles are scarce and the relationship of photodegradation with self-cleaning properties remains unclear.[20] These properties have been independently explored on tungsten-loaded TiO_2 colloids ($W-TiO_2$) and over films deposited on model substrates, such as glass.[21−26] Although the role of tungsten is not fully understood, it is recognized that when included in the TiO_2 lattice or segregated on the TiO_2 surface the photoactivity might be extended to the visible range.[27,28] It is also claimed that the surface becomes more hydrophilic,[29] and the generation of reactive oxidative species (ROS) during irradiation (mainly hydroxyl $^{\bullet}OH$) increases,[30] which may induce disruption of cellular processes, leading to bacteria inactivation.[31,32] However, substitution of Ti(IV) by W(VI) in the TiO_2 lattice or $W(VI)-TiO_2$ composites depends on the synthesis pathway, and results from different authors are not strictly comparable.

In previous works, we demonstrated that W-loaded TiO_2 ($W-TiO_2$) nanoparticles synthesized via a sol−gel route exhibit good photocatalytic activity in suspension toward crystal violet (CV) degradation.[33,34] Here, we propose the use of $W-TiO_2$ coatings synthesized via surface sol−gel on commercial glazed ceramic tiles as self-cleaning and antimicrobial surfaces for indoor applications. We focus on the microstructure and surface composition in order to establish the role of tungsten on self-cleaning performance measured as wettability, photodegradation of CV, and inactivation of *Escherichia coli* (DH5α) under different light sources. Finally, from these results, we develop a prototype of self-cleaning tile entirely processed in an industrial plant with a promising performance under artificial light and sunlight.

2. RESULTS

2.1. Microstructure of $W-TiO_2$ Films. The film morphology, surface area, and TiO_2 crystallinity over the tile surface are considered important parameters to tune wettability, photocatalytic response, and antimicrobial activity.[11] The surface sol−gel process provides a complete coverage of the tile by TiO_2 or $W-TiO_2$ nanoparticles, as shown in scanning electron microscopy (SEM) images (Figure 1).

Increase in annealing temperature at fixed W(VI) loading leads to an increase in grain size that decreases the surface area, whereas at fixed annealing temperature, the grain size decreases with the W(VI) content incrementing the surface area, as summarized in Table 1. The particle size distribution becomes broader as the annealing temperature increases. TiO_2 coatings (without W) show higher variation than tungsten-loaded ones (see grain size histograms in Figure S2 and insets in Figure 1). At the same annealing temperature, the distribution narrows as the tungsten content increases (Figure S3).

X-ray diffraction (XRD) patterns for different compositions and annealing temperatures are shown in Figure 2. All samples exhibit the (101) diffraction peak of anatase at 25.3° (JCPDS 21-1272). For unloaded TiO_2, this peak becomes narrower with the increase of annealing temperature, indicating that anatase crystalline domains grow with temperature. The rutile phase contribution (JCPDS 21-1276) begins to appear at 600 °C and reaches a rutile/anatase ratio of 0.63 at 800 °C. These results are in good agreement with the reported ART temperature.[35] When tungsten is added, the rutile peak at

DOI: 10.1021/acsomega.8b03339
ACS Omega 2018, 3, 17629−17636

Table 1. Anatase Crystallite Sizes and Mean Grain Sizes for W−TiO_2 Films at Different Annealing Temperatures

sample	anatase crystallite size (±10)% (nm)[a]	mean grain size (nm)[b]
W0 400 °C	8	(14 ± 3)
W5 400 °C	6	(9 ± 2)
W0 600 °C	15	(22 ± 5)
W1 600 °C	16	(18 ± 5)
W2 600 °C	12	(15 ± 2)
W5 600 °C	11	(12 ± 2)
W0 800 °C	22	(52 ± 20)
W5 800 °C	16	(32 ± 5)

[a]Measured with the Scherrer equation using the (101) peak for anatase. [b]Determined from SEM images.

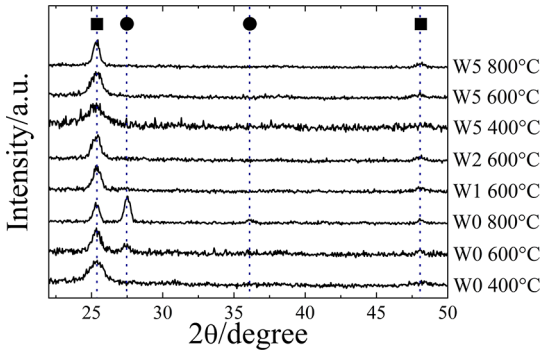

Figure 2. XRD patterns for the films. Peaks pointed as (■) or (●) correspond to anatase and rutile TiO_2 crystalline phases, respectively.

27° is absent even at 800 °C. Moreover, the anatase (101) peak is broader than the corresponding peak for unloaded TiO_2, revealing a more amorphous structure or smaller crystallites, suggesting that tungsten inhibits TiO_2 crystallization. Table 1 presents the size of crystalline domains estimated from XRD data using Scherrer's equation. For W0, there is an increase in crystallite size from 8 to 22 nm as the temperature increases from 400 to 800 °C, whereas for W5, the crystallite size increases from 6 to 16 nm. The absence of crystalline WO_3 peaks (e.g., JCPDS 43-0679 for orthorhombic or 43-1035 for monoclinic phase) suggests that WO_x moieties are present either as oligomers or as small crystallites unable to diffract X-rays.

The surface tungsten content for different loading and annealing temperature was determined by X-ray photoelectron spectroscopy (XPS) (representative XPS spectra are shown in Figure S4). The location and full width at half-maximum (fwhm) of the bands remain unaltered for all samples, and the relative intensity of Ti and W bands changes with the W concentration or temperature. The calculated surface W/Ti ratio ($[W/Ti]_s$) (for details, see Section 5.3) at constant annealing temperature is higher than the nominal ratio (Figure 3a), whereas at constant nominal W/Ti, the $[W/Ti]_s$ ratio increases with the annealing temperature and reaches a constant value above 600 °C (Figure 3b). The $[W/Ti]_s$ is higher than expected for a homogeneous bulk distribution of W(VI) on TiO_2, denoting that WO_x species are preferentially located at the titania surface. Either at constant temperature or at constant W loading, the maximum $[W/Ti]_s$ ratio is 12.5%. Analogous results were obtained using tungsten ethoxide as the precursor, indicating that the location of WO_x species on the surface is independent of the tungsten source (see Figure S5).

2.2. Water Contact Angle. Water contact angle (WCA) measurements before, immediately after, and 24 h after UV irradiation for the samples annealed at 600 °C are shown in Figure 4. The TiO_2 film is a more hydrophilic surface than the naked tile, as noticed by the WCA decrease of approximately 20°. Hydrophilicity is even greater as the W content increases (column A in Figure 4). Immediately after irradiation with *black light* (column B), WCA drops to 0° for all coated tiles with a slow recovery toward initial conditions when samples are stored in the dark (column C). Thus, the presence of tungsten in TiO_2-coated tiles improves their wettability.

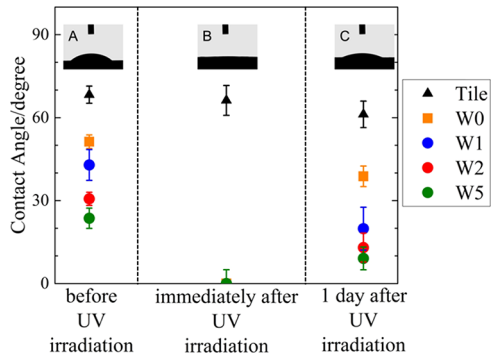

Figure 4. WCA for the W−TiO_2 films deposited on glazed ceramic tiles. WCA for samples annealed at 600 °C was measured before, immediately after, and 24 h after UV irradiation. Insets A−C are representative photographs of the water drop over the W5-coated tile taken during the WCA measurement at each condition.

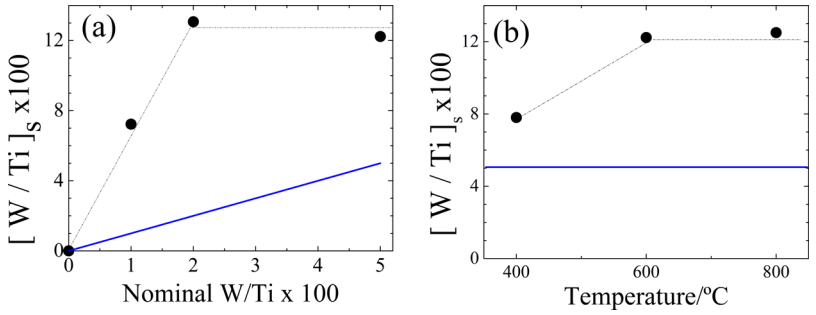

Figure 3. Surface W/Ti ratio calculated from the XPS spectra of films supported on silicon (a) variable W loading at constant annealing temperature (600 °C) and (b) 5% W loading at variable temperature. The filled circles represent $[W/Ti]_s$ calculated from XPS spectra, and the lines correspond to the expected value for a W(IV) homogeneous distribution.

DOI: 10.1021/acsomega.8b03339
ACS Omega 2018, 3, 17629−17636

2.3. CV Photodegradation. Photocatalytic activity was evaluated by analyzing the decomposition rate of CV spread on the coated tiles. CV adsorption leads to different surface complexes whose distribution depends on the film annealing temperature, as revealed by the distribution of absorption bands in the 450−700 nm range (Figure S6). When irradiated under *vis light*, the intensity of these bands decreases because of CV photodegradation. However, the slight absorbance increment in the 400−470 nm range suggests that CV was not completely mineralized.[36]

Figure 5 shows pseudo-first-order kinetic curves for CV photodegradation, determined from the peak area ratios in the

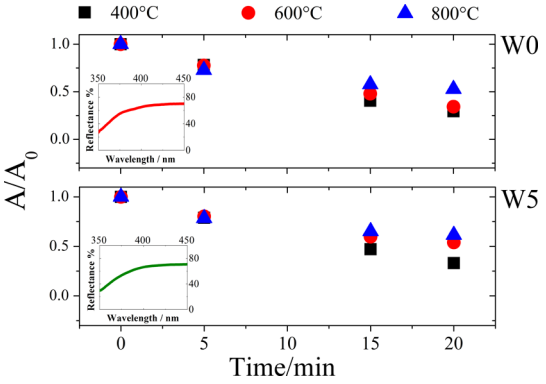

Figure 5. Photocatalytic degradation of violet crystal under *vis light* with tiles covered with W0 or W5 annealed at 400 °C (squares), 600 °C (circles), and 800 °C (triangles).

400−700 nm range. It represents the performance of TiO_2 (W0) and W−TiO_2 (W5)-coated tiles annealed at 400, 600, or 800 °C when irradiated with *vis light*. Data obtained for other W(VI) loadings and irradiation sources are shown in Figures S7−S9 of the Supporting Information. In all cases, an increase in the annealing temperature produces a lower dye photodegradation rate. Minor differences are found when varying the coating composition. This is in good agreement with the negligible shift of absorption onset determined from reflectance spectra (Figure S10).

Table 2 compiles the rate constants derived from kinetic data and the photonic efficiency calculated as the ratio between

Table 2. Pseudo-First-Order Constants and Photonic Efficiency under Each Illumination Source for W0 and W5 Samples

	k (s^{-1}) × 10^{-3}			photonic efficiency (Φ) × 10^{-3}		
sample	*vis*	*white*	*black*	*vis*	*white*	*black*
W0 400 °C	1.017	0.080	0.717	0.14	0.35	1.98
W0 600 °C	0.850	0.055	0.850	0.12	0.24	2.35
W0 800 °C	0.550	0.085	0.300	0.08	0.37	0.83
W5 400 °C	0.883	0.025	0.733	0.13	0.11	2.03
W5 600 °C	0.533	0.065	1.483	0.08	0.28	4.11
W5 800 °C	0.417	0.075	0.333	0.06	0.33	0.92

the initial reaction rate and photon flux on the exposed tile area. As expected, the photonic efficiency under *black light* is higher than the obtained efficiency when samples are illuminated in the visible region, using either *vis light* or *white light* source. The rate constant decreases when the annealing temperature reaches 800 °C. Moreover, at each annealing temperature, the photonic efficiency under the visible light is independent of the coating composition. This result provides evidence that in the unloaded TiO_2 film, the synthesis pathway and thermal treatment induce photoactivity in the visible range because of surface defects. It should be noted that in oxygen-deficient TiO_2 surfaces, the broadening for Ti 2p bands toward lower binding energies—characteristic for Ti^{3+} species—is barely detected;[37−39] thus, the density of defects such as O vacancies or Ti^{3+} in our samples should be low.

2.4. Antimicrobial Activity. The antimicrobial activity tests with *E. coli* under different light sources are shown in Figure 6 for W0 and W5 coatings. Results are normalized to the uncoated tile, which also exhibit a decrease of colony-forming units (CFU) under the same irradiation conditions, probably because of cell dehydration. Under *black light*, both samples W0 and W5 annealed at 600 °C present a similar decrease in bacterial content (Figure 6a) compared to control tiles. In contrast, under *white light*, the bacterial viability is 45% lower when 5% tungsten is included in the coating compared to bare TiO_2 (Figure 6b).

2.5. Preliminary Manufacturing in an Industrial Plant. Using the optimal synthesis conditions determined for maximum wettability, photocatalysis, and reduction of bacterial viability, we designed and produced W−TiO_2-covered tiles with 5% W(VI) in a plant. Coatings were deposited in the enamel line and treated in a roller furnace at 600 °C (Figure S11a). Uniform, colorless, and adherent coatings (pass abrasion test class 2) with small anatase grains were obtained. CV spread on these tiles is bleached after 40 min exposure to sunlight (Figure S11b).

3. DISCUSSION

From the results presented in the previous section, the incorporation of W(VI) to titania produces an enhancement of wettability (Figure 4) and antimicrobial activity under visible light (Figure 6) but has negligible effect on the photodegradation of CV (Figure 5). The wettability and antimicrobial response are correlated with the surface excess of W(VI) at the titania nanoparticle surface that inhibits particle growth and stabilizes the anatase phase, as discussed below.

The sol−gel synthesis of W−TiO_2 nanoparticles involves hydrolysis and condensation at pH = 2. At this pH, Ti(O−*i*-Pr)$_4$ quickly forms TiO_2 particles with a positive surface charge,[40] and ammonium metatungstate (AMT) gives negatively charged, stable, and discrete units (WO_x), such as α-Keggin or β-Keggin structures among other polytungstates.[41] Therefore, negatively charged species (WO_x) are adsorbed onto fresh and positively charged TiO_2 nanoparticles.

The surface excess of W determined from XPS (Figure 3) results from a migration of tungsten at the particle surface when the annealing temperature reaches 600 °C. This WO_x excess at the surface is a consequence of merging of titania building blocks, producing an increase in the grain size and promoting WO_x migration to the particle surface, as schematized in Figure 7.

The saturation value of $[W/Ti]_s$ = 12.5%—reached either at constant temperature increasing nominal W at 5% W by increasing temperature—implies that the TiO_2 surface charge limits WO_x adsorption in the sol, and any nonadsorbed WO_x is removed by dialysis (the dialysis membrane filters particles up to 5 nm diameter). The limited WO_x adsorption is

DOI: 10.1021/acsomega.8b03339
ACS Omega 2018, 3, 17629−17636

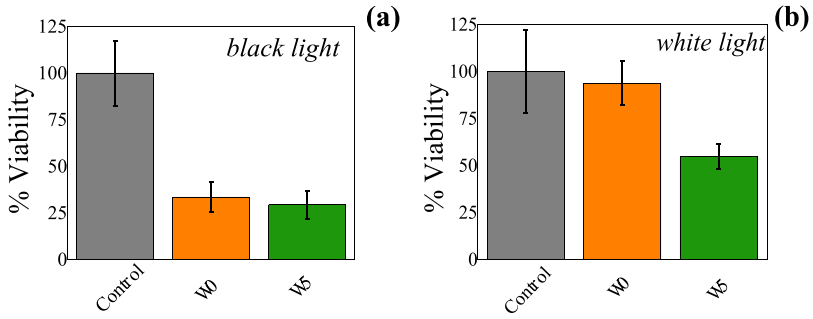

Figure 6. *E. coli* inactivation by (a) *black light* for 10 min and (b) *white light* for 30 min over the ceramic tile (control), ceramic tile with the titania film (W0), and ceramic tile with the titania film with 5% mol/mol of tungsten (W5), both annealed at 600 °C.

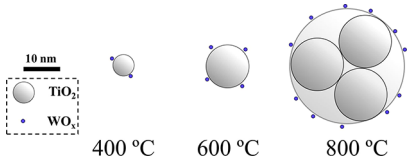

Figure 7. Scheme of coarsening and sintering of W−TiO_2 nanoparticles with the annealing temperature.

corroborated as similar results are obtained using a tungsten precursor with different hydrolysis behavior, such as W-ethoxide (Figure S5). The presence of WO_x at the titania surface has several consequences. First, it reduces the coarsening as it hinders the contact between titania building blocks. Second, it inhibits merging of anatase crystallites with the appropriate orientation for ART[42] (i.e., with octahedral units tilted in opposite directions) that is confirmed by the absence of rutile, even at 800 °C (Figure 2). Third, in order to maintain electroneutrality, WO_x eliminates oxygen vacancies at the titania surface.[43]

The addition of WO_x on the titania surface leads to lower WCA before UV irradiation. This effect is related to the change in surface charge, as other parameters involved in wettability such as crystal structure and surface roughness[44,45] are unchanged with the W content for samples annealed at 600 °C. The hydrophilicity enhancement under UV light has been attributed to chemisorbed ROS, such as $O_2^{-\bullet}$ and $HO^{\bullet}$ produced by photogenerated holes.[46] The fact that tiles coated with W−TiO_2 or unloaded TiO_2 become superhydrophilic under *black light* indicates that in both cases the surface defect density is enough to produce chemisorbed ROS. Storage in dark induces recovery of the original WCA because of the replacement of adsorbed ROS by the atmospheric oxygen. In addition, the formation of WO_x species on TiO_2 increases the surface acidity[47] that stabilizes surface hydroxyl groups allowing to retain wettability after storage in the dark. This change in surface charge as W loading increases enables the possibility of tuning wettability with the W content.

Although the antimicrobial behavior of TiO_2 is not yet well understood, it is widely accepted that under UV light the biocidal activity is correlated with the concentration of ROS, which triggers a disruption of the cell wall giving rise to deleterious alterations of metabolic and communication processes.[48,49] Moreover, the interaction of cells with the surface affects these processes, leading to biofilm formation.[50] Within this framework, the incomplete inactivation of *E. coli* on TiO_2 and W−TiO_2-coated tiles under *black light* (Figure 6a) is caused by the low rate of ROS production combined with the stress response under low power irradiation (10 min, 210 μW cm^{-2}).[51] Under *white light*, W−TiO_2 coatings exhibit an improved antimicrobial effect compared to TiO_2. This behavior is again related to a more negative surface, giving higher ROS concentration[30] and inhibiting the formation of biofilms,[52] thus reducing the bacterial viability.

CV photocatalytic degradation on TiO_2 follows a complex mechanism involving ring opening and demethylation, leading to discoloration and the formation of recalcitrant byproducts,[53] as revealed by the complex evolution of adsorbed CV reflectance spectra in Figure S6. It is worth to note that dye sensitization could affect its photodegradation, but as CV is not an efficient sensitizing molecule for TiO_2,[54] this can be disregarded. The W(VI) addition has little effect on the TiO_2 photoactivity toward CV photodegradation, although it has been reported that tungsten plays a beneficial role—especially under visible light—because of reduction of band gap and generation of defect sites.[17] The slight variations on the reflectance spectra (Figures 5 and S10) rule out changes in the electronic structure. On the other hand, the band gap of WO_x oligomers falls in the 3.5−4.0 eV range;[55] thus, their contribution to photodegradation can be neglected. For all coatings, as expected, the photonic efficiency (Table 2) when irradiated with *black light* is higher than those irradiated with *vis* or *white light* and photoactivity decreases when the annealing temperature increases. These results show that neither crystallinity nor surface area plays an important role in the CV photodegradation, as the W−TiO_2 coatings did not exhibit rutile (Figure 2) and grains are significantly smaller than for unloaded TiO_2 (Figure 1, Table 1). When excited in the UV region, complexes formed by CV adsorption on sites with unsaturated coordination act as deep hole traps, and then photodegradation should mainly proceed by direct hole transfer instead of the Langmuir−Hinshelwood mechanism.[56] Under this rationale, titania films prepared by this surface sol−gel approach should exhibit uncoordinated surface sites that are not affected by W(VI) addition, as the photodegradation rate with *black light* is nearly independent from the W content. The dye photodegradation rate under *vis light* and *white light* for unloaded coatings supports the idea of surface sites with localized energy levels in the band gap inducing TiO_2 absorption in the 400−600 nm range. Thus, surface point defects induced by hydrolysis and condensation of Ti precursors—probably unaffected by W(VI)— play a major role in the CV photodegradation.[57]

4. CONCLUSIONS

The main conclusion of this work is that self-cleaning properties depend on surface defects rather than on crystalline

DOI: 10.1021/acsomega.8b03339
ACS Omega 2018, 3, 17629−17636

structures or grain sizes. At least two kinds of defects are involved in the self-cleaning performance: (i) those that affect the surface electronic density and modify surface acidity that can be tuned with W(VI) and (ii) those related to unsaturated coordination of Ti atoms at the surface that are determined by the synthesis pathway of TiO_2 building blocks. The first group depends on the concentration of WO_x at the surface and participates in ROS chemisorption, improving wettability and the antimicrobial activity under *vis light*. The second group is involved in photodegradation by direct hole transfer and remains unaltered when WO_x specimens are added. Although the antimicrobial activity and dye photodegradation rate are far to be optimal, the surface sol−gel synthesis pathway in the acid media of W−TiO_2 coatings is promising to be applicable in a factory with current technology for tile's processing, thus enabling a strategy for massive production of self-cleaning ceramic tiles.

5. EXPERIMENTAL SECTION

5.1. Reagents. Titanium(IV) isopropoxide (97%) and CV (>90%) were purchased from Sigma-Aldrich. Nitric acid was Baker Analyzed—ACS reagent 69−70%. AMT $[(NH_4)_{10}W_{12}O_{41}\cdot 7H_2O]$ was prepared by neutralization of tungstic acid (Aldrich, 99%) with ammonia (Anedra). Ultrapure water (Milli-Q, 18 MΩ) was used in all experiments.

5.2. Synthesis of TiO_2 Films. TiO_2 and 1, 2, or 5% mol/mol tungsten/TiO_2 were prepared by a sol−gel process. Samples were named as W*X*, where *X* indicates the nominal tungsten (W) molar percentage with respect to the total cationic content. The necessary amount of AMT was dissolved in 180 mL of water with 1.8 mL of nitric acid contained in an open spherical flask. Titanium isopropoxide (15 mL) was slowly incorporated to the acid solution under strong stirring. A white suspension was obtained immediately and was heated at 80 °C for 30 min; the alcohol produced as a consequence of the alkoxide hydrolysis was partially evaporated in this step. Finally, the suspension was refluxed at 80 °C for 2 h until total peptization and dialyzed against water until pH = 3.5 (Spectra/Por 3 dialysis membrane tubing 3.500 MWCO regenerated cellulose).

The obtained sols were sprayed on white glazed ceramic tiles Milano provided by Cooperativa de Trabajo FASINPAT. A 0.30 g/cm^2 of sol (ca. 6 mg/cm^2 TiO_2) was deposited with each application. The sprayed tiles were air-dried and annealed at 400, 600, or 800 °C for 30 min using a 5 °C/min ramp. The process (spraying, drying, and annealing) was repeated three times in total for obtaining a homogeneous coating. For comparison purposes, films were also prepared using tungsten ethoxide as the organic precursor.[33]

5.3. Films Morphology and Tungsten Species Characterization. The crystalline structure was determined by XRD with a Siemens D-5000 equipment using a Cu Kα radiation source filtered with a graphite monochromator (λ = 1.5406 Å). For this analysis, the film was deposited on a silicon wafer by the same procedure. Crystalline domain size was calculated using Scherrer's equation, considering the shape factor typical for spherical crystallites (K = 0.94) and the fwhm at maximum diffraction angle for the [101] crystallographic direction in anatase.

The morphology of the films was observed with a field emission gun SEM (FEG-SEM) (Zeiss Supra 40) instrument operated at 4 kV. The mean grain size was obtained by processing images with ImageJ (>40 grains for each image).

Electron photoemission spectra (XPS) for samples prepared from W-ethoxide or metatungstate precursors were obtained with a vacuum generator (VG) CLAMP 3 (0.3 eV resolution) operating in the constant analyzer energy mode in an ultrahigh vacuum chamber (background pressure, $p \approx 10^{-9}$ mbar, room temperature) using Al Kα line (VG XR X-ray source, $h\nu$ = 1486.6 eV, width 0.85 eV). Films were deposited on silicon wafers for these experiments. Quantification of W/Ti atomic ratio at the surface ($[W/Ti]_s$) was done taking into account the area of Ti 2p and W 4d bands and their corresponding cross sections.[58] Although W 4d bands are broader and with lower intensity than W 4f bands, they were considered for quantification in order to avoid interference from the Ti 3p signal that overlaps W 4f bands.

5.4. Water Contact Angle. The hydrophilicity of the coatings was determined from WCA measurements performed in a ramé-hart 200 standard contact angle goniometer with DROPimage standard software. Results are averaged over six or more fresh spots. Measurements were performed in air at room temperature (22−23 °C). The samples were irradiated with a 38 W UV light (Philips) with an irradiance of 210 μW cm^{-2} (λ_{max} = 350 nm) for 60 min.

5.5. Photocatalytic Degradation of CV. The photocatalytic performance of coated tiles was determined by spreading a CV solution and exposing it to a light source under controlled humidity at (55 ± 5)%. In a typical experiment, a CV solution in isopropanol (100 mg L^{-1}) was dropped into the tile (70 μL per dm^2), dried at ambient conditions, and exposed to light. At the specified times, illumination was shut down and a diffuse reflectance spectrum was measured (Ocean Optics spectrometer with integrating sphere). Quantification of CV on the surface was performed through the area of the diffuse reflectance spectra in the 400−700 nm range.

Three different light sources were used. (i) A 150 W XBO Osram Xe lamp with a cell filled with $CuSO_4$ solution (IR filter for minimizing heating) and a polycarbonate sheet (UV cutoff) placed between the lamp and the tile. This configuration with continuum emission between 400 and 600 nm and 2700 μW cm^{-2} (λ_{max} = 520 nm) irradiance is referred to as *vis light*. (ii) A 40 W white fluorescent tube (Philips) with an irradiance of 90 μW cm^{-2} (λ_{max} = 520 nm), in the text called *white light*. (iii) A 38 W UV light (Philips) with an irradiance of 210 μW cm^{-2} (λ_{max} = 350 nm), named *black light*. Irradiance values were measured at the position of the tile with a Coherent radiometer using the appropriate UV or vis sensor set at the mentioned wavelength parenthesis. In the case of the measurement at 520 nm, a band-pass filter was used (2 mm Schott VG14). The emission spectra of the lamps are shown in the Supporting Information (Figure S1).

Photonic efficiencies (Φ) under each light source were calculated as the ratio between CV disappearance rate and incident photon flux. For this, the initial rate was calculated considering a pseudo-first-order kinetic constant (mol m^{-2} s^{-1}) and the photonic flux (I_o, einstein m^{-2} s^{-1}) was estimated for each lamp transforming the power density into flux values in the λ_{max}.

5.6. Antimicrobial Activity. The antimicrobial activity was tested using *E. coli* (DH5α) as the model microorganism. Stock bacterial suspensions were grown at (37 ± 1) °C under orbital agitation (120 rpm) in a liquid Tryptone Soya (TS) medium. To avoid further cellular division of bacteria, an isotonic liquid medium without carbon source was used for work dilutions. Appropriate dilution of stock suspension was

DOI: 10.1021/acsomega.8b03339
ACS Omega 2018, 3, 17629−17636

adjusted by optical density (600 nm) to obtain 5×10^4 UFC/mL. A homogeneous distribution of bacterial suspensions was obtained after dispersing 4 μL per cm^2 over each tile surface. The tiles were placed in a chamber at 25 °C and irradiated at 20 cm for 10 min with black light or 30 min with white light. After irradiation, samples were analyzed for cell viability by contact spotting of samples onto a semisolid culture medium (TS) and incubation at 37 °C for 24 h. The number of viable bacteria per tile was obtained after incubation by conventional counting of CFU on agar plates. Each experiment was done with six replicates.

■ ASSOCIATED CONTENT

Supporting Information

The Supporting Information is available free of charge on the ACS Publications website at DOI: 10.1021/acsomega.8b03339.

Emission spectra of the light sources, particle size histograms, XPS spectra for W0 and W5 samples, surface W/Ti ratio varying tungsten precursor, CV reflectance spectra, photocatalytic performance under different light sources, reflectance spectra for the covered and uncovered ceramic tiles, and pictures of the ceramic tile coating scale-up (PDF)

■ AUTHOR INFORMATION

Corresponding Authors

*E-mail: diego.onna@qi.fcen.uba.ar (D.O.).
*E-mail: keyla@qi.fcen.uba.ar (K.M.F.).
*E-mail: sarabil@qi.fcen.uba.ar (S.A.B.).

ORCID

Diego Onna: 0000-0002-3158-1915
Fernando Alvarez: 0000-0002-9393-1298

Author Contributions

The manuscript was written through contributions of all authors. All authors have given approval to the final version of the manuscript.

Notes

The authors declare no competing financial interest.

■ ACKNOWLEDGMENTS

This work was supported by ANPCyT PICT-2012-1167, UBACyT 20020170200298BA, and CONICET-PIP_11220170100289CO. We are indebted to the program "Exactas con la Sociedad" that promoted this cooperative work with FASINPAT, including DO and CS student fellowships. R.J.C. and S.A.B. thank Jorge Bermudez and Carlos Diaz for their technical support at FASINPAT-Zanon (Parque Industrial Neuquén) and Carolina Ortega for the first successful coated tiles. M.P., M.C.M., R.J.C., and S.A.B. are members of CONICET.

■ REFERENCES

(1) Kirchnerova, J.; Herrera Cohen, M.-L.; Guy, C.; Klvana, D. Photocatalytic Oxidation of N-Butanol under Fluorescent Visible Light Lamp over Commercial TiO_2 (Hombicat UV100 and Degussa P25). *Appl. Catal., A* **2005**, *282*, 321−332.

(2) Calvo, M. E.; Candal, R. J.; Bilmes, S. A. Photooxidation of Organic Mixtures on Biased TiO_2 Films. *Environ. Sci. Technol.* **2001**, *35*, 4132−4138.

(3) Parkin, I. P.; Palgrave, R. G. Self-Cleaning Coatings. *J. Mater. Chem.* **2005**, *15*, 1689.

(4) Blossey, R. Self-cleaning surfaces—virtual realities. *Nat. Mater.* **2003**, *2*, 301−306.

(5) Fagan, R.; McCormack, D. E.; Dionysiou, D. D.; Pillai, S. C. A Review of Solar and Visible Light Active TiO_2 Photocatalysis for Treating Bacteria, Cyanotoxins and Contaminants of Emerging Concern. *Mater. Sci. Semicond. Process.* **2016**, *42*, 2−14.

(6) Cedillo-González, E. I.; Riccò, R.; Montorsi, M.; Montorsi, M.; Falcaro, P.; Siligardi, C. Self-Cleaning Glass Prepared from a Commercial TiO_2 Nano-Dispersion and Its Photocatalytic Performance under Common Anthropogenic and Atmospheric Factors. *Build. Environ.* **2014**, *71*, 7−14.

(7) Faraldos, M.; Kropp, R.; Anderson, M. A.; Sobolev, K. Photocatalytic hydrophobic concrete coatings to combat air pollution. *Catal. Today* **2016**, *259*, 228−236.

(8) Radeka, M.; Markov, S.; Lončar, E.; Rudić, O.; Vučetić, S.; Ranogajec, J. Photocatalytic Effects of TiO_2 Mesoporous Coating Immobilized on Clay Roofing Tiles. *J. Eur. Ceram. Soc.* **2014**, *34*, 127−136.

(9) Murugan, K.; Subasri, R.; Rao, T. N.; Gandhi, A. S.; Murty, B. S. Synthesis, Characterization and Demonstration of Self-Cleaning TiO_2 Coatings on Glass and Glazed Ceramic Tiles. *Prog. Org. Coating* **2013**, *76*, 1756−1760.

(10) Bianchi, C. L.; Colombo, E.; Gatto, S.; Stucchi, M.; Cerrato, G.; Morandi, S.; Capucci, V. Photocatalytic Degradation of Dyes in Water with Micro-Sized TiO_2 as Powder or Coated on Porcelain-Grès Tiles. *J. Photochem. Photobiol., A* **2014**, *280*, 27−31.

(11) Fujishima, A.; Zhang, X.; Tryk, D. TiO_2 Photocatalysis and Related Surface Phenomena. *Surf. Sci. Rep.* **2008**, *63*, 515−582.

(12) Nowotny, M. K.; Sheppard, L. R.; Bak, T.; Nowotny, J. Defect Chemistry of Titanium Dioxide. Application of Defect Engineering in Processing of TiO_2 -Based Photocatalysts. *J. Phys. Chem. C* **2008**, *112*, 5275−5300.

(13) Pan, X.; Yang, M.-Q.; Fu, X.; Zhang, N.; Xu, Y.-J. Defective TiO_2 with Oxygen Vacancies: Synthesis, Properties and Photocatalytic Applications. *Nanoscale* **2013**, *5*, 3601.

(14) Madras, G.; McCoy, B. J.; Navrotsky, A. Kinetic Model for TiO_2 Polymorphic Transformation from Anatase to Rutile. *J. Am. Ceram. Soc.* **2007**, *90*, 250−255.

(15) Banerjee, S.; Dionysiou, D. D.; Pillai, S. C. Self-Cleaning Applications of TiO_2 by Photo-Induced Hydrophilicity and Photocatalysis. *Appl. Catal., B* **2015**, *176−177*, 396−428.

(16) Hanaor, D. A. H.; Sorrell, C. C. Review of the Anatase to Rutile Phase Transformation. *J. Mater. Sci.* **2010**, *46*, 855−874.

(17) Di Paola, A.; Marcì, G.; Palmisano, L.; Schiavello, M.; Uosaki, K.; Ikeda, S.; Ohtani, B. Preparation of Polycrystalline TiO_2 Photocatalysts Impregnated with Various Transition Metal Ions: Characterization and Photocatalytic Activity for the Degradation of 4-Nitrophenol. *J. Phys. Chem. B* **2002**, *106*, 637−645.

(18) Xu, H.; Ouyang, S.; Liu, L.; Reunchan, P.; Umezawa, N.; Ye, J. Recent Advances in TiO_2 -Based Photocatalysis. *J. Mater. Chem. A* **2014**, *2*, 12642.

(19) Kenevey, K.; Morris, M. A.; Cunningham, J.; Ferrand, G. Stabilization of Anatase by Tungsten Introduced to the Titania Lattice by Sol-Gel and Impregnation Techniques. *Key Eng. Mater.* **1996**, *118−119*, 303−312.

(20) da Silva, A. L.; Dondi, M.; Raimondo, M.; Hotza, D. Photocatalytic Ceramic Tiles: Challenges and Technological Solutions. *J. Eur. Ceram. Soc.* **2018**, *38*, 1002−1017.

(21) Rampaul, A.; Parkin, I. P.; O'Neill, S. A.; DeSouza, J.; Mills, A.; Elliott, N. Titania and Tungsten Doped Titania Thin Films on Glass; Active Photocatalysts. *Polyhedron* **2003**, *22*, 35−44.

(22) Lin, C.-L.; Chen, Y.-W.; Chen, E. Preparation and characterization of electrochromic tungsten oxide-titania composite thin films with different tungsten/titanium ratios. *Thin Solid Films* **2014**, *556*, 48−53.

(23) Patrocinio, A. O. T.; Paula, L. F.; Paniago, R. M.; Freitag, J.; Bahnemann, D. W. Layer-by-Layer TiO_2/ WO_3 Thin Films As Efficient Photocatalytic Self-Cleaning Surfaces. *ACS Appl. Mater. Interfaces* **2014**, *6*, 16859−16866.

DOI: 10.1021/acsomega.8b03339
ACS Omega 2018, 3, 17629−17636

(24) Vaiano, V.; Sarno, G.; Sannino, D.; Ciambelli, P. Photocatalytic and Antistain Properties of Ceramic Tiles Functionalized with Tungsten-Doped TiO_2. *Chem. Eng. Trans.* **2014**, *39*, 499−504.
(25) Chen, H.-K.; Chen, W.-F.; Koshy, P.; Adabifiroozjaei, E.; Liu, R.; Sheppard, L. R.; Sorrell, C. C. Effect of Tungsten-Doping on the Properties and Photocatalytic Performance of Titania Thin Films on Glass Substrates. *J. Taiwan Inst. Chem. Eng.* **2016**, *67*, 202−210.
(26) Tadić, N.; Stojadinović, S.; Radić, N.; Grbić, B.; Vasilić, R. Characterization and Photocatalytic Properties of Tungsten Doped TiO_2 Coatings on Aluminum Obtained by Plasma Electrolytic Oxidation. *Surf. Coat. Technol.* **2016**, *305*, 192−199.
(27) Li, X. Z.; Li, F. B.; Yang, C. L.; Ge, W. K. Photocatalytic Activity of WOx-TiO_2 under Visible Light Irradiation. *J. Photochem. Photobiol., A* **2001**, *141*, 209−217.
(28) Khan, H.; Rigamonti, M. G.; Patience, G. S.; Boffito, D. C. Spray Dried TiO_2 /WO_3 Heterostructure for Photocatalytic Applications with Residual Activity in the Dark. *Appl. Catal., B* **2018**, *226*, 311−323.
(29) Lebarbier, V.; Clet, G.; Houalla, M. Relations between Structure, Acidity, and Activity of WOx/ TiO_2 : Influence of the Initial State of the Support, Titanium Oxyhydroxide, or Titanium Oxide. *J. Phys. Chem. B* **2006**, *110*, 22608−22617.
(30) Meng, Z.-D.; Zhu, L.; Ullah, K.; Ye, S.; Oh, W.-C. Detection of Oxygen Species Generated by WO_3 Modification Fullerene/TiO_2 in the Degradation of 1,5-Diphenyl Carbazide. *Mater. Res. Bull.* **2014**, *56*, 45−53.
(31) Cho, M.; Chung, H.; Choi, W.; Yoon, J. Linear Correlation between Inactivation of E. Coli and OH Radical Concentration in TiO_2 Photocatalytic Disinfection. *Water Res.* **2004**, *38*, 1069−1077.
(32) Huang, Z.; Maness, P.-C.; Blake, D. M.; Wolfrum, E. J.; Smolinski, S. L.; Jacoby, W. A. Bactericidal Mode of Titanium Dioxide Photocatalysis. *J. Photochem. Photobiol., A* **2000**, *130*, 163−170.
(33) Alcober, C.; Alvarez, F.; Bilmes, S. A.; Candal, R. J. Photochromic W-TiO_2 Membranes. *J. Mater. Sci. Lett.* **2002**, *21*, 501−504.
(34) Couselo, N.; García Einschlag, F. S.; Candal, R. J.; Jobbágy, M. Tungsten-Doped TiO_2 vs Pure TiO_2 Photocatalysts: Effects on Photobleaching Kinetics and Mechanism. *J. Phys. Chem. C* **2008**, *112*, 1094−1100.
(35) Nolan, N. T.; Seery, M. K.; Pillai, S. C. Spectroscopic Investigation of the Anatase-to-Rutile Transformation of Sol−Gel-Synthesized TiO_2 Photocatalysts. *J. Phys. Chem. C* **2009**, *113*, 16151−16157.
(36) Couselo, N.; García Einschlag, F. S.; Candal, R. J.; Jobbágy, M. Tungsten-Doped TiO_2 vs Pure TiO_2 Photocatalysts: Effects on Photobleaching Kinetics and Mechanism. *J. Phys. Chem. C* **2008**, *112*, 1094−1100.
(37) Pan, J.-M.; Maschhoff, B. L.; Diebold, U.; Madey, T. E. Interaction of Water, Oxygen, and Hydrogen with TiO_2 (110) Surfaces Having Different Defect Densities. *J. Vac. Sci. Technol., A* **1992**, *10*, 2470−2476.
(38) Bilmes, S. A.; Mandelbaum, P.; Alvarez, F.; Victoria, N. M. Surface and Electronic Structure of Titanium Dioxide Photocatalysts. *J. Phys. Chem. B* **2000**, *104*, 9851−9858.
(39) Sathasivam, S.; Bhachu, D. S.; Lu, Y.; Chadwick, N.; Althabaiti, S. A.; Alyoubi, A. O.; Basahel, S. N.; Carmalt, C. J.; Parkin, I. P. Tungsten Doped TiO_2 with Enhanced Photocatalytic and Optoelectrical Properties via Aerosol Assisted Chemical Vapor Deposition. *Sci. Rep.* **2015**, *5*, 10952.
(40) Bischoff, B. L.; Anderson, M. A. Peptization Process in the Sol-Gel Preparation of Porous Anatase (TiO_2). *Chem. Mater.* **1995**, *7*, 1772−1778.
(41) Cruywagen, J. J. Protonation, Oligomerization, and Condensation Reactions of Vanadate(V), Molybdate(vi), and Tungstate-(vi). *Adv. Inorg. Chem.* **1999**, *49*, 127−182.
(42) Kubacka, A.; Iglesias-Juez, A.; di Michiel, M.; Becerro, A. I.; Fernández-García, M. Morphological and Structural Behavior of TiO_2 Nanoparticles in the Presence of WO_3: Crystallization of the Oxide Composite System. *Phys. Chem. Chem. Phys.* **2014**, *16*, 19540−19549.
(43) Onfroy, T.; Lebarbier, V.; Clet, G.; Houalla, M. Quantitative Relationship between the Nature of Surface Species and the Catalytic Activity of Tungsten Oxides Supported on Crystallized Titania. *J. Mol. Catal. A: Chem.* **2010**, *318*, 1−7.
(44) Shibata, T.; Irie, H.; Ohmori, M.; Nakajima, A.; Watanabe, T.; Hashimoto, K. Comparison of Photochemical Properties of Brookite and Anatase TiO_2 Films. *Phys. Chem. Chem. Phys.* **2004**, *6*, 1359.
(45) Quéré, D. Wetting and Roughness. *Annu. Rev. Mater. Res.* **2008**, *38*, 71−99.
(46) Wang, R.; Hashimoto, K.; Fujishima, A.; Chikuni, M.; Kojima, E.; Kitamura, A.; Shimohigoshi, M.; Watanabe, T. Light-Induced Amphiphilic Surfaces. *Nature* **1997**, *388*, 431−432.
(47) Akurati, K. K.; Vital, A.; Dellemann, J.-P.; Michalow, K.; Graule, T.; Ferri, D.; Baiker, A. Flame-Made WO_3/TiO_2 Nanoparticles: Relation between Surface Acidity, Structure and Photocatalytic Activity. *Appl. Catal., B* **2008**, *79*, 53−62.
(48) McKenzie, K.; Maclean, M.; Grant, M. H.; Ramakrishnan, P.; MacGregor, S. J.; Anderson, J. G. The effects of 405 nm light on bacterial membrane integrity determined by salt and bile tolerance assays, leakage of UV-absorbing material and SYTOX green labelling. *Microbiology* **2016**, *162*, 1680−1688.
(49) Kubacka, A.; Diez, M. S.; Rojo, D.; Bargiela, R.; Ciordia, S.; Zapico, I.; Albar, J. P.; Barbas, C.; Martins dos Santos, V. A. P.; Fernández-García, M.; et al. Understanding the Antimicrobial Mechanism of TiO_2-Based Nanocomposite Films in a Pathogenic Bacterium. *Sci. Rep.* **2014**, *4*, 4134.
(50) Wolfrum, E. J.; Huang, J.; Blake, D. M.; Maness, P.-C.; Huang, Z.; Fiest, J.; Jacoby, W. A. Photocatalytic Oxidation of Bacteria, Bacterial and Fungal Spores, and Model Biofilm Components to Carbon Dioxide on Titanium Dioxide-Coated Surfaces. *Environ. Sci. Technol.* **2002**, *36*, 3412−3419.
(51) Mitoraj, D.; Jańczyk, A.; Strus, M.; Kisch, H.; Stochel, G.; Heczko, P. B.; Macyk, W. Visible Light Inactivation of Bacteria and Fungi by Modified Titanium Dioxide. *Photochem. Photobiol. Sci.* **2007**, *6*, 642−648.
(52) Gottenbos, B. Antimicrobial Effects of Positively Charged Surfaces on Adhering Gram-Positive and Gram-Negative Bacteria. *J. Antimicrob. Chemother.* **2001**, *48*, 7−13.
(53) Chen, C.; Mai, F.; Chen, K.; Wu, C.; Lu, C. Photocatalyzed N-de-Methylation and Degradation of Crystal Violet in Titania Dispersions under UV Irradiation. *Dyes Pigm.* **2007**, *75*, 434−442.
(54) Lai, W. H.; Su, Y. H.; Teoh, L. G.; Hon, M. H. Commercial and Natural Dyes as Photosensitizers for a Water-Based Dye-Sensitized Solar Cell Loaded with Gold Nanoparticles. *J. Photochem. Photobiol., A* **2008**, *195*, 307−313.
(55) Ross-Medgaarden, E. I.; Wachs, I. E. Structural Determination of Bulk and Surface Tungsten Oxides with UV−vis Diffuse Reflectance Spectroscopy and Raman Spectroscopy. *J. Phys. Chem. C* **2007**, *111*, 15089−15099.
(56) Regazzoni, A. E.; Mandelbaum, P.; Matsuyoshi, M.; Schiller, S.; Bilmes, S. A.; Blesa, M. A. Adsorption and Photooxidation of Salicylic Acid on Titanium Dioxide: A Surface Complexation Description. *Langmuir* **1998**, *14*, 868−874.
(57) Diebold, U. The Surface Science of Titanium Dioxide. *Surf. Sci. Rep.* **2003**, *48*, 53−229.
(58) Briggs, D.; Seah, M. P. *Practical Surface Analysis, Auger and X-Ray Photoelectron Spectroscopy*; Practical Surface Analysis; Wiley, 1996.

DOI: 10.1021/acsomega.8b03339
ACS Omega 2018, 3, 17629−17636